X-RAY SPECTROMETRY, VOL. 23, 254–260 (1994)

Peak-to-Background Method for Standardless Electron Microprobe Analysis of Particles

J. Trincavelli* and R. Van Grieken
Department of Chemistry, University of Antwerp (UIA), B-2610 Antwerp–Wilrijk, Belgium

A peak-to-background method was implemented for standardless electron microprobe analysis of bulk samples and particles. First, a study on the choice of the beam entry point was performed; the region of the particle closest to the detector proved to be the most convenient. Then, a very simple algorithm, which does not require any kind of standard, was developed for particle analysis. This method was tested for glass standard particles and the results were compared with those given by other methods; the proposed standardless approach appeared to yield very satisfactory results.

INTRODUCTION

The characterization of individual particles by electron probe microanalysis (EPMA) presents several problems due to size and shape effects, which do not occur in bulk samples. On the one hand, for particle sizes below the interaction volume of the electrons, the characteristic intensity generated within the particle is only a fraction of the intensity generated in a bulk sample of the same composition. On the other hand, the irregular shape of a particle makes it very difficult to take into account correctly the attenuation of characteristic photons between their generation sites and the particle surface.

Owing to the important applications of quantitative particle microanalysis during the last 20 years, a number of methods have been proposed to overcome these problems. These methods include normalization of bulk ZAF results,[1] normalization to the beam raster area,[2] the modified P factor method,[3] geometric modelling of the particle shape,[4] Monte Carlo simulations[5] and the peak-to-background (P/B) method.[6–8] This work will focus on the last method.

The P/B method assumes that both characteristic and bremsstrahlung photons originate from the same region in the sample and that bremsstrahlung photons are emitted isotropically, like the characteristic photons. Assuming this approximation to be valid, the peak-to-background ratio for a given element i is the same for a particle and a bulk sample:

$$\frac{P_p}{B_p} = \frac{P_b}{B_b} \tag{1}$$

From this equation, the peak intensity P_b of a bulk sample with the same composition as the particle can be expressed as a function of the peak and background intensities measured on the particle and as a function of B_b, which can be estimated from an iterative process. For P_b it is possible to perform a conventional ZAF correction, in which the inaccuracies of the approximation assumed in Eqn (1) should be taken into account, as it was pointed out in the original paper of Small *et al.*[6]

Recently, Lábár and Török[8] used the P/B method in a standardless procedure. According to this method:

$$C_i = k_i \mathbf{Z}_c R_c \mathbf{A}_c \mathbf{F}_c \tag{2}$$

where

$$k_i = \frac{(P/B)_i^{\,x}}{(P/B)_i^{\,s}} \tag{3}$$

The indices x and s correspond to the unknown sample and a pure standard, respectively. In Eqn (2), C_i represents the mass concentration of element i in the unknown sample and the factors $\mathbf{Z}_c$, R_c, $\mathbf{A}_c$ and $\mathbf{F}_c$ are atomic number, backscattering, absorption and fluorescence corrections, respectively. As pointed out by the authors, the main effect corresponds to the atomic number factor, the other three being second-order corrections (particularly, the fluorescence correction is omitted in the original paper).

In this work, an alternative standardless method is proposed. Applications of this method will be discussed in this paper for both bulk samples and particles.

DESCRIPTION OF THE MODEL

The detected characteristic intensity P_i of a given line from element i in the sample can be written as

$$P_i = C_i(\mathbf{ZAF})_i \omega_i(fr)_i \varepsilon_i I \frac{\Delta\Omega}{4\pi} \tag{4}$$

where **Z**, **A** and **F** indicate the atomic number, absorption and fluorescence corrections, ω is the fluorescence yield for the considered atomic (sub)shell, (fr) is the fraction of the observed line with respect to all the lines

* On leave from Universidad Nacional de Córdoba, República Argentina, Consejo Nacional de Investigaciones Científicas y Técnicas de la República Argentina.

CCC 0049–8246/94/060254–07

Received 10 November 1993
Accepted 15 August 1994

originated in the same (sub)shell, ε is the detector efficiency, I is the primary beam intensity and $\Delta\Omega$ is the solid angle subtended by the detector.

The bremsstrahlung intensity B at the energy E_i corresponding to the line considered can be expressed as

$$B = f(\bar{Z}, E_i, E_0)\mathbf{A}\varepsilon I \frac{\Delta\Omega}{4\pi} \tag{5}$$

where f describes the generation of bremsstrahlung, being a function of the mean atomic number $\bar{Z}$ of the sample, the incidence energy E_0 and the energy E_i; the other factors are the same as in Eqn (4). From Eqns (4) and (5), an expression for the mass concentration C_i can be obtained:

$$C_i = \frac{P_i}{B_i} \frac{f(\bar{Z}, E_i, E_0)}{[\mathbf{ZF}\omega(fr)]_i} \tag{6}$$

As can be seen, the efficiency and geometric factors related to detection, and also the primary beam intensity, are cancelled out; in addition, the absorption factor is considered the same for characteristic and continuum radiation. In addition to its simplicity, the advantage of this model, applicable for both particles and bulk samples, is that the P/B ratio appears only once and not twice as in the first formulation[6] or in the method of Lábár and Török.[8] Therefore, the large uncertainties related to experimental deconvolution of peaks (especially in the low-energy range) and the problems in predicting the bremsstrahlung spectrum are, in principle, reduced (when considering P/B ratios, there is, nevertheless, the possibility of fortuitous error cancellation). On the other hand the (not always well known) fluorescence yields and the line fractions are required; in some cases this is another important source of uncertainty. The line fractions used in Eqn (6) are obtained from a polynomial fitting to Scofield's[9] data, the fluorescence yields are taken from Hubbell[10] for the K shell and from Miyagawa *et al.*[11] for the L_{III} shell. For the function $f(\bar{Z}, E_i, E_0)$ in Eqn (6), both the modifications of Lifshin[12] and Reed[13] to Kramers'[14] equation were tested. After fitting the empirical coefficients present in both equations using a set of spectra from pure elements, Reed's model was found to be the best. Thus, the function $f(\bar{Z}, E_i, E_0)$ can be expressed as

$$f(\bar{Z}, E_i, E_0) = a\bar{Z} \frac{E_0 - E_i}{E_i^{(1-b)}} \tag{7}$$

with

$$a = \ln(-5.086 \times 10^{-14}\bar{Z} + 2.0264 \times 10^{-11}) \tag{8}$$

and

$$b = 0.002\bar{Z} - 0.2719 \tag{9}$$

For the atomic number correction, the model proposed by Riveros *et al.*[15] was used. This model is based on the Gaussian ionization distribution function proposed by Packwood and Brown.[16] When the quantification procedure was applied to bulk samples, Reed's fluorescence correction model[17] was employed.

One of the common problems in analysing small particles with a P/B method is the influence of the bremsstrahlung originated in the substrate. It is possible to express the bremsstrahlung intensity B_i generated for a given energy E_i as composed by a contribution B_i^x of the sample itself and other B_i^0 from the substrate:

$$B_i = B_i^x + A_i^0 B_i^0 \tag{10}$$

where A_i^0 takes into account the absorption of the bremsstrahlung photons of energy E_i generated in the substrate, up to the place of generation of the bremsstrahlung photons of the same energy within the particle. Based on Eqn (5), by neglecting the weak dependence of parameter b on $\bar{Z}$ in Eqn (7), as seen in Eqn (9), one can write

$$\frac{B_i^0}{B_i^x} = \frac{a^0\bar{Z}^0}{a^x\bar{Z}^x} \tag{11}$$

where the indices 0 and x refer to the substrate and sample, respectively. Combining Eqn (10) with Eqn (11) yields

$$B_i = B_i^x\left(1 + A_i^0 \frac{a^0\bar{Z}^0}{a^x\bar{Z}^x}\right) \tag{12}$$

When the beam entry point is in the particle side nearest to the detector, the factor A_i^0 is close to unity, since most of the photons originated in the substrate, which are emitted towards the detector, do not enter into the particle because of the detection geometry. Thus, for this particular choice for the beam entry point, the factor in parentheses in Eqn (12) is almost independent of the photon energy and, therefore, it will be cancelled out in Eqn (6) after the normalization step. As can be seen from Eqn (12), this approximation is particularly good when the mean atomic number of the sample is much greater than the mean atomic number of the substrate.

Another problem is quantifying particles by EPMA is to take into account properly the enhancement produced by fluorescence. For small particles, the interaction volume of secondary fluorescence is usually larger than the particle itself. In this case, it is not possible to use a conventional fluorescence correction factor, since only a fraction of the expected enhancement will actually be produced. For example, according to Small,[18] in a Ni–10% Fe alloy, only 50% of Ni Kα photons fluorescing Fe Kα photons are produced within a semisphere of radius 20 μm. Hence, in a particle of diameter, say, 3 μm, the enhancement produced by characteristic fluorescence is not very important. In addition, the continuum fluorescence is also a 'long-range effect,' exceeding even the range for characteristic fluorescence. Because of the aforementioned reasons, in the present method, the fluorescence correction will be neglected for small particles, such as those considered in this paper, i.e. $\mathbf{F} = 1$ in Eqn (6).

EXPERIMENTAL

Four glass particle standard spheres (NBS K227, K309, K411 and K961) were analysed using a JEOL-733 electron microprobe, equipped with a Tracor energy-dispersive x-ray analysis system. Spectra were acquired with a Si(Li) detector, for incident beam energies of 25

keV at current intensities of 2 nA and for counting times ranging from 200–400 s. The detector forms an angle of 40° with the plane of the sample holder. The particles were deposited on an organic substrate and covered by evaporation with a carbon coating in order to make the samples conductive. After data acquisition, the background was subtracted by means of the AXIL[19] spectral analysis package.

RESULTS

Influence of the point of electron beam entry into a particle

As mentioned above, the present model assumes that characteristic and bremsstrahlung photons are originated in the same region of the sample. Figure 1 shows qualitatively the 1.5 keV x-ray cross-section variation with path length for a 20 keV electron incident on a pure aluminium sample; as can be seen, the cross-sections for both characteristic and continuum radiation are very similar in the early stages of the electron trajectory. If the entry point of the electron beam is on the side of the particle nearest to the detector, then x-ray absorption will act in favour of the radiation generated within these surface layers, minimizing the inaccuracies of the approximation assumed.

In addition, as can be seen from Fig. 2, the absorption correction becomes smaller when the entry point of the beam is closer to the detector. This is very important because the absorption correction is usually the most prominent and therefore it introduces most ot the uncertainties in a microanalysis quantification.

In order to study the influence of the entry point of the beam on the performance of the method, spectra were recorded for a single particle, varying the incidence point from the furthest position with respect to the detector (position 1) to the closest (position 10), along

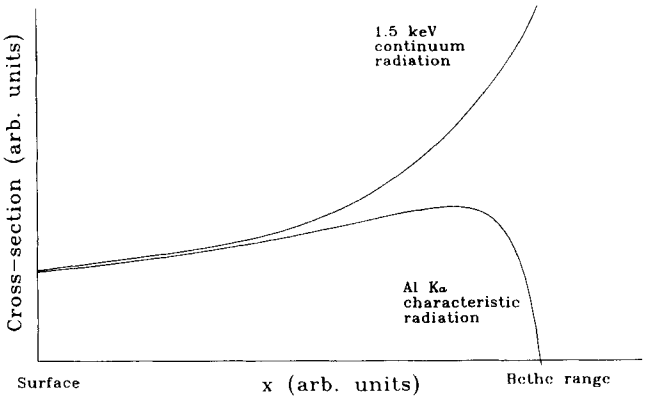

Figure 1. Cross-section for the production of 1.5 keV characteristic and continuum x-rays in Al as a function of the electron penetration x.

the diameter of the particle parallel to the detection direction.

In a multi-component particle, the absorption effect is more important for the light elements; hence, when the beam entry point is far from the detector, the concentration of these elements would be underestimated by using an algorithm for bulk samples. Therefore, in this position of the entry point, the heavy elements would be overestimated in comparison with the light elements, since the concentrations are normalized to 100%. In addition, by increasing the 'position number' from 1–10 (except for the glass K961, for which only nine beam entry points were considered), the deviation of the bulk algorithm from the certified concentrations should decrease continuously. All these features can be observed from Figs 3–5, in which the concentrations of certain elements given by Riveros *et al.*'s model[15] for bulk samples are plotted against the position of the beam entry point for three of the four different kind of particles analysed. In Figs 3–6, the concentrations given by the standardless P/B method are plotted. As can be seen, the improvement achieved is very significant.

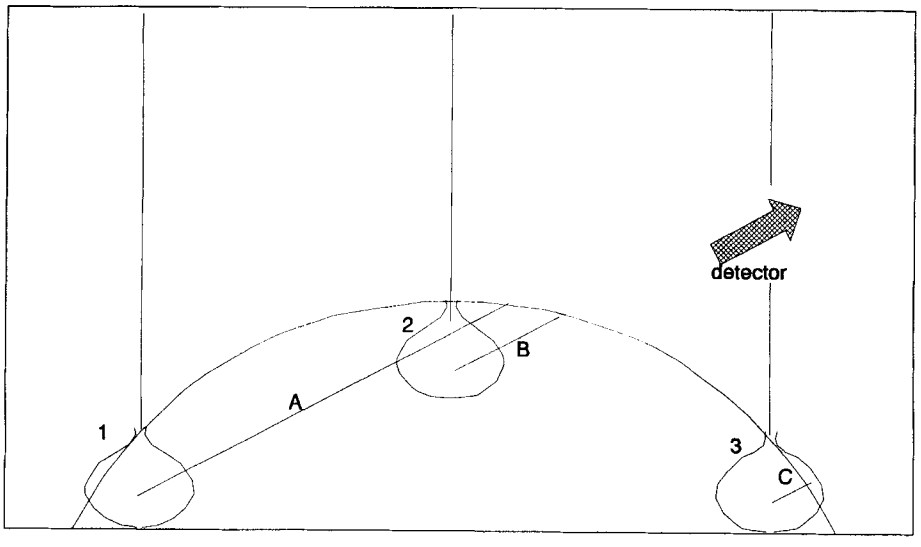

Figure 2. Detection geometry for a spherical particle. As an example, points 1, 2 and 3 indicate three different positions for the entry point of the beam (indicated as a vertical line) on the particle surface; the three tear-shaped areas are the regions of electron beam penetration in the three cases; A, B, and C are the corresponding exit paths of the characteristic x-rays towards the detector.

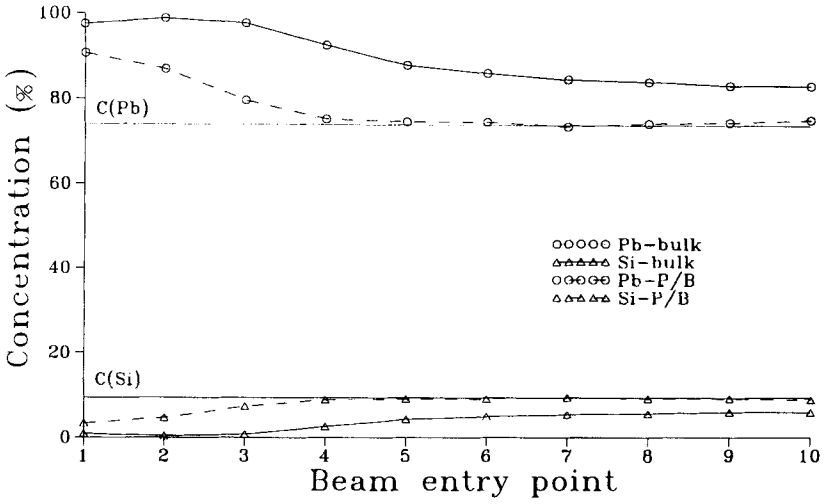

Figure 3. Pb and Si concentrations for standard K227 by means of both bulk and standardless particle algorithms as a function of the beam entry point.

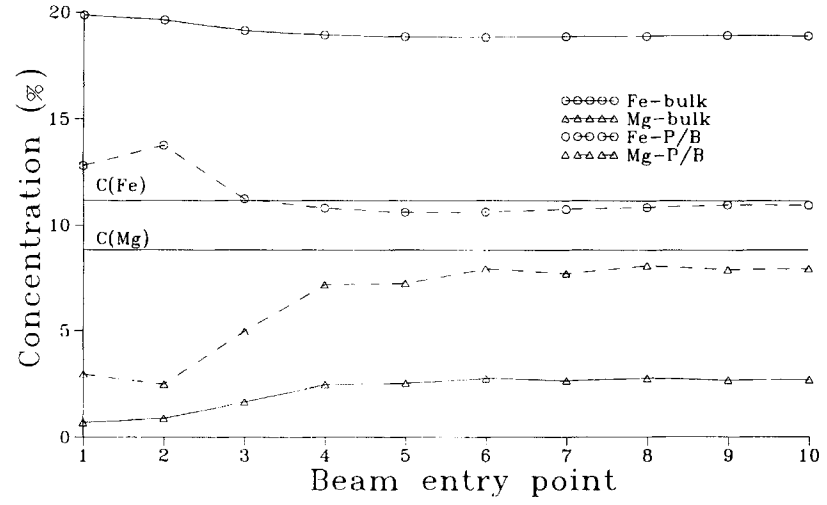

Figure 4. Fe and Mg concentrations for standard K961 by means of both bulk and standardless particle algorithms as a function of the beam entry point.

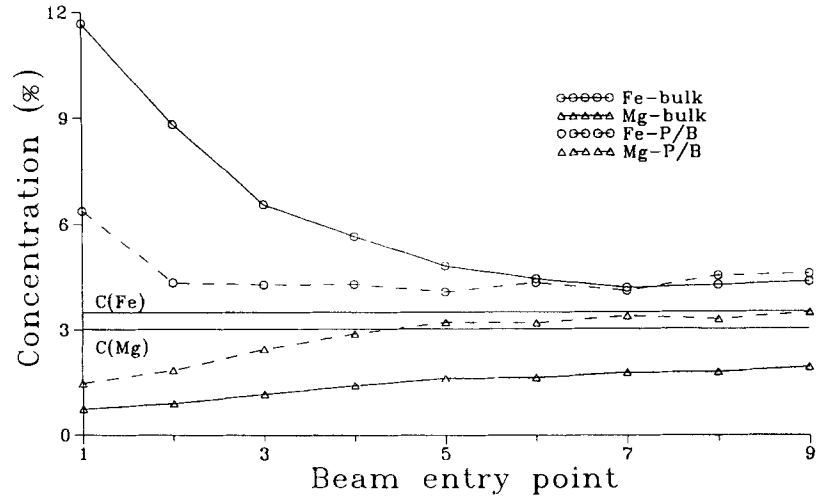

Figure 5. Fe and Mg concentrations for standard K411 by means of both bulk and standardless particle algorithms as a function of the beam entry point.

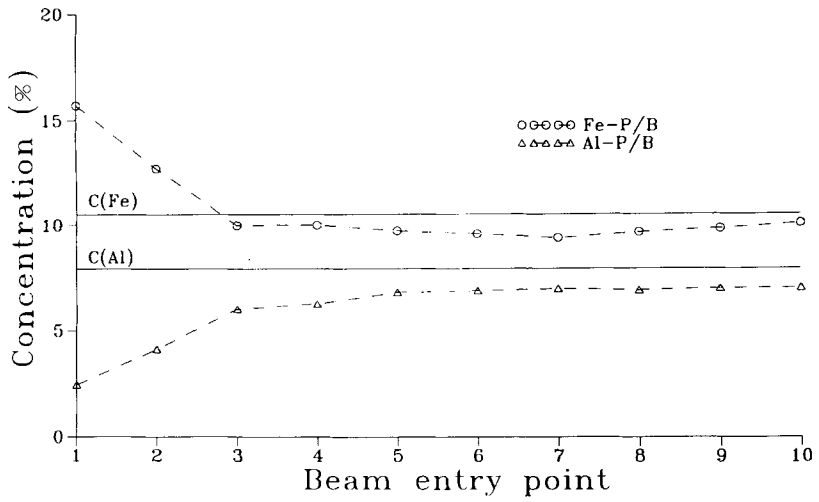

Figure 6. Fe and Al concentrations for standard K309 by means of the standardless particle algorithm as a function of the beam entry point.

Nevertheless, as was expected, the approximation that characteristic and bremsstrahlung photons are originated in the same region of the sample is fulfilled only when the beam entry point is in the particle side nearest to the detector. Similar results were also obtained by Statham and Pawley[7] considering peak-to-background ratios and peak areas for three different beam entry points normalized to data corresponding to a raster scan just covering the particle.

Applicability of the model

For each of the four glasses considered, the analysed particles were grouped into four different types according to their diameter: 1–2 μm (group 1), 2–3 μm (group 2), 3–4 μm (group 3) and 4–7 μm (group 4). About ten spectra were acquired for each of these groups and the concentrations obtained were averaged in each case.

In order to express the discrepancies between calculated C_i and nominal concentrations C_i^n, a parameter ε is defined as a weighted average of the relative errors of all the elements analysed in the sample multiplied by 100, the weight factors being the respective concentrations. In this way, the most abundant elements in the sample are considered as the most important. Hence the parameter ε can be expressed as

$$\varepsilon = \frac{\sum |C_i^n - C_i|}{\sum C_i^n} \times 100 \qquad (13)$$

Results of the standardless model applied to two standard bulk alloys are given in Table 1. As can be seen, in both cases the parameter ε indicates a deviation of 6% from the certified concentrations. The results obtained for the four particle standards analysed are presented in Tables 2–5. In all cases oxygen was calculated by stoichiometry and therefore it was not taken into account in the calculation of ε. For the case of the standard K961, a comparison with results given by Lábár and Török[8] was performed in Table 5. They divided their data into three groups, namely for the particles of 1.3 μm (corresponding to our group 1), 2.9 μm (corresponding to our group 2) and 30 μm (approaching the case of bulk samples, like our group 4); ε_L indicates the parameter ε calculated for their results. In this last case, elements that are hardly detectable such as P and Na are not considered (as Lábár and Török did not). The large root mean square (r.m.s.) error for these two elements indicates that the problem is in the spectra themselves and not in the correction models. In addition, Mn is also not considered in order to compare

Table 1. Concentrations (%) obtained by the *P/B* standardless method compared with certified values for two standard bulk alloys

	Bulk-66		Bulk-37	
Element	*P/B*	Certified	*P/B*	Certified
Cr	17.56	15.64	22.91	23.4
Mn	0.65	0.42	0.64	0.38
Fe	77.61	80.60	24.81	26.5
Ni	2.62	2.16	44.45	43.5
Cu	0.33	0.162	2.04	1.75
Si	0.96	0.545	0.55	3.32
Mo	0.26	0.164	4.27	2.73
Ti			0.93	0.75
ε	6%		6%	

Table 2. Concentrations (%) obtained by the *P/B* standardless method compared with certified values for the particle standard K227[a]

Element	Group 1	Group 2	Group 3	Group 4	Certified
Pb	75.1 ± 2.6	71.4 ± 1.3	71.5 ± 2.3	69.7 ± 2.4	74.3
Si	9.0 ± 1.0	10.4 ± 0.5	10.3 ± 0.8	11.0 ± 0.9	9.4
O	15.8 ± 1.7	18.2 ± 0.8	18.1 ± 1.5	19.3 ± 1.5	16.3
ε	1.4%	5%	4%	7%	

[a] Particles were divided into four groups according to their diameters. Each averaged value displayed corresponds to about 10 particles.

Table 3. Concentrations (%) obtained by the *P/B* standardless method compared with certified values for the particle standard K309[a]

Element	Group 1	Group 2	Group 3	Group 4	Certified
Si	18.4 ± 0.6	17.7 ± 0.5	17.7 ± 0.2	17.9 ± 0.2	18.7
Al	7.6 ± 0.4	7.3 ± 0.3	7.4 ± 0.2	7.4 ± 0.2	7.9
Ca	11.4 ± 0.6	12.5 ± 0.5	12.5 ± 0.4	12.6 ± 0.2	10.7
Fe	10.3 ± 1.0	10.5 ± 0.3	10.2 ± 0.3	9.7 ± 0.2	10.5
Ba	14.1 ± 1.0	15.3 ± 1.2	15.3 ± 0.5	15.4 ± 0.3	13.4
O	38.1 ± 1.2	36.7 ± 1.0	36.7 ± 0.4	37.1 ± 0.4	38.8
ε	3%	9%	9%	10%	

[a] Particles were divided into four groups according to their diameters. Each averaged value displayed corresponds to about 10 particles.

with Lábár and Török, who did not give results for this element.

As can be seen from Tables 2–5, the results are always within 10% (except for K411 particles larger than 4 μm, where $\varepsilon = 12\%$). For particles smaller than 2 μm, the discrepancies are within 7%. There is a slow trend for increasing discrepancies with increasing particle size; this is probably because, for large particles, the x-rays are always not originated from a region close to the surface, even when the beam entry point is in the particle side nearest to the detector. Therefore, the regions of generation of characteristic and bremsstrahlung photons are different (see previous section). In addition, fluorescence correction is no longer negligible as assumed. Finally, as shown in Table 5, our method presents better results than those given by Lábár and Török for the three particle sizes compared. It must be emphasized that comparison is made for only one kind of particles and testing a wider set of samples would be of interest.

Table 4. Concentrations (%) obtained by the *P/B* standardless method compared with certified values for the particle standard K411[a]

Element	Group 1	Group 2	Group 3	Group 4	Certified
Fe	10.8 ± 0.9	11.0 ± 0.7	10.7 ± 0.7	10.3 ± 0.5	11.2
Mg	9.7 ± 1.8	9.1 ± 1.1	9.0 ± 1.1	9.7 ± 0.6	8.8
Si	27.7 ± 2.7	26.0 ± 1.2	27.1 ± 1.7	28.7 ± 0.8	25.4
Ca	11.4 ± 1.3	12.9 ± 1.2	13.3 ± 0.6	12.8 ± 1.5	11.1
O	40.3 ± 3.3	40.9 ± 2.5	39.8 ± 2.4	38.4 ± 1.7	43.5
ε	7%	5%	8%	12%	

[a] Particles were divided into four groups according to their diameters. Each averaged value displayed corresponds to about 10 particles.

CONCLUSIONS

A simple model which does not need standards was developed for the quantification of particles in the range 1–7 μm and also for bulk samples. The results show discrepancies generally within 10% for all particle sizes, within 7% for particles between 1 and 2 μm and within 6% for two bulk alloys. In addition, the model compares favourably with another standardless model for particle analysis recently published.[8] It would be interesting to test the model with a wider set of particles, especially for non-spherical particles, in order to confirm the convenience of the beam entry position selected in the particle side nearest to the detector. Finally, the anisotropy of bremsstrahlung generation and a fluorescence correction for particles should be included in the model.

Acknowledgement

J.T. acknowledges financial support from the Consejo Nacional de Investigaciones Científicas y Técnicas de la República Argentina.

Table 5. Concentrations (%) obtained by the *P/B* standardless method compared with certified values for the particle standard K961[a]

Element	Group 1	Group 2	Group 3	Group 4	Certified
Si	30.2 ± 0.4	29.7 ± 0.2	29.3 ± 0.2	29.6 ± 0.2	29.9
Ca	4.0 ± 0.3	4.5 ± 0.2	5.2 ± 0.2	5.0 ± 0.1	3.6
Mg	3.5 ± 0.2	3.5 ± 0.2	3.4 ± 0.2	3.4 ± 0.1	3.0
Al	6.4 ± 0.2	6.3 ± 0.3	6.2 ± 0.2	6.2 ± 0.1	5.8
Ti	1.4 ± 0.1	1.5 ± 0.1	1.7 ± 0.1	1.6 ± 0.1	1.2
P	0.05 ± 0.07	0.03 ± 0.02	0.02 ± 0.01	0.04 ± 0.05	0.2
Fe	3.5 ± 0.2	3.7 ± 0.2	3.8 ± 0.1	3.7 ± 0.1	3.5
Mn	0.3 ± 0.1	0.3 ± 0.1	0.3 ± 0.1	0.3 ± 0.1	0.3
Na	1.1 ± 0.3	1.2 ± 0.3	1.1 ± 0.4	0.8 ± 0.3	3.0
K	2.1 ± 0.2	2.3 ± 0.2	2.8 ± 0.2	2.8 ± 0.2	2.5
O	47.5 ± 0.6	46.8 ± 0.3	46.1 ± 0.3	46.5 ± 0.3	46.9
ε	5%	6%	8%	7%	
ε_L	10%	7%		10%	

[a] Particles were divided into four groups according to their diameters. Each averaged value displayed corresponds to about 10 particles.

REFERENCES

1. F. Wright, P. Hodge and C. Langway, *J. Geophys. Res.* **68**, 5575 (1963).
2. J. Gavrilovic, *NBS Spec. Publ.* No. 533, 21 (1980).
3. G. Aden and P. Buseck, *Microbeam Anal.* 195 (1983).
4. J. Armstrong and P. Buseck, *Anal. Chem.* **47**, 2178 (1975).
5. Y. Ho, J. Chen, M. Hu and X. Wang, *Scanning Microsc.* **1**, 943 (1987).
6. J. Small, K. Heinrich, D. Newbury and R. Myklebust, *Scanning Electron Microsc.* **2**, 807 (1979).
7. P. Statham and J. Pawley, *Scanning Electron Microsc.* **1**, 469 (1978).
8. J. Lábár and S. Török, *X-Ray Spectrom.* **4**, 21 (1992).
9. J. Scofield, *Phys. Rev. A* **10**, 1507 (1974).
10. J. Hubbel, NISTIR 89-4144, National Institute of Standards and Technology, Gaithersburg Md. (1989).
11. Y. Miyagawa, S. Nakamura and S. Miyagawa, *Nucl. Instrum. Methods Phys. Res.* **B30**, 115 (1988).
12. E. Lifshin, in *Proceedings of the IXth Conference of the Microbeam Analysis Society, Ottawa, Canada*, p. 53. (1974).
13. S. Reed, *X-Ray Spectrom.* **2**, 16 (1975).
14. H. Kramers, *Philos. Mag.* **46**, 836 (1923).
15. J. Riveros, G. Castellano and J. Trincavelli, *Mikrochim. Acta (Suppl.)* **12**, 99 (1992).
16. R. Packwood and J. Brown, *X-Ray Spectrom.* **10**, 138 (1981).
17. S. Reed, Br. J. Appl. Phys. **16**, 913 (1965).
18. J. Small, *Scanning Electron Microsc.* **1**, 447 (1981).
19. P. Van Espen, K. Janssens and J. Nobels, *Chemometr. Intell. Lab. Syst.* **1**, 109 (1986).